ELSEVIER

Biophysical Chemistry 98 (2002) 301–312

Biophysical Chemistry

www.elsevier.com/locate/bpc

The conformation of dehydroalanine in short homopeptides: molecular dynamics simulations of a 6-residue chain

David Zanuy[a], Jordi Casanovas[b,*], Carlos Alemán[a,1,*]

[a]*Departament d'Enginyeria Quimica, ETSEIB, Universitat Politècnica de Catalunya, Diagonal 647, Barcelona E-08028, Spain*
[b]*Departament de Quimica, Escola Universitària Politècnica, Universitat de Lleida, c/Jaume II no. 69, Lleida E-25001, Spain*

Received 15 October 2001; received in revised form 8 April 2002; accepted 9 April 2002

Abstract

A molecular dynamics study about the conformational preferences in a chloroform solution of a homo-oligomer constituted by six residues of dehydroalanine is presented. For this purpose, two sets of force-field parameters and explicit solvent molecules have been used. Furthermore, ab initio calculations have been performed in order to estimate ^{1}[H]-NMR chemical shifts. Results have been compared with experimental data.

Keywords: Dehydroalanine; Molecular dynamics; Force-field; Extended conformation; Helical conformation; GIAO calculations

1. Introduction

Dehydroalanine (ΔAla) is an α,β-unsaturated amino acid commonly found in a number of naturally occurring peptide antibiotics and in some proteins [1]. The double bond of the side chain provides to the residue a very defined conformational behavior. The potential energy hypersurface of the ΔAla-containing dipeptide was investigated some years ago by the authors using ab initio quantum mechanical calculations [2]. The results indicated that the extended, also denoted C_5 (five-membered) hydrogen bonded system is the lowest energy conformation. More recently, Thormann and Hofmann reached the same conclusion in a systematic study about the conformational properties of diamides containing dehydro amino acids [3].

On the other hand, a number of theoretical analyses on ΔAla homo-oligomers, denoted $(\Delta Ala)_n$, have been reported. Both force-field [4,5] and quantum mechanical [6,7] calculations predict that the fully extended conformation is the most stable for homo-oligomers with a small number of residues, while the 3_{10}-helix becomes favored for a large number of residues. The number of residues required for the conformational transition extended $\rightarrow 3_{10}$-helix depends on the theoretical method used for the calculations. Thus, semi-empirical and ab initio calculations indicated that the 3_{10}-helix is the most stable conformation in the gas-phase for

*Corresponding author. Tel.: +34-973-702783; fax: +34-973-702-702.

E-mail address: jcasanovas@quimica.udl.es (J. Casanovas), aleman@eq.upc.es (C. Alemán).

[1] Also at: Tel.: +34-93-401883; fax: +34-93-4016600.

0301-4622/02/$ - see front matter
PII: S0301-4622(02)00108-4

$n \geq 8$ and $n \geq 6$, respectively. Quantum mechanical calculations on ΔAla-containing peptides allowed us to find another interesting result [2]. This is the significant variation in molecular geometry upon conformational changes. Thus, in the helical conformation, the bond angle $<N-C^{\alpha}-C(O)$ takes a large value (120°), in agreement with the trigonal configuration of the C^{α} atom, whereas in the extended conformation, such an angle adopts a tetrahedral value (109.5°). This narrow value was recently confirmed in peptides containing one, two and three ΔAla residues, which were studied by X-ray crystallography [8].

In a very recent work, Toniolo and coworkers reported a conformational study in a chloroform solution of the homo-oligomeric series *p*BrBz–$(\Delta Ala)_n$–OMe (where *p*BrBz and OMe are *p*-bromobenzoyl and methoxy, respectively) with *n* ranging from 1 to 6 [8]. FTIR absorption and ^{1}[H]-NMR results indicated that the fully extended is the conformation preferred by ΔAla homopeptides up to hexamer level. These data point out that the threshold value predicted by HF/4-31G calculations for the conformational transition ($n \geq 6$) is underestimated [6]. This deficiency can be attributed to several reasons, such as the poor quality of the molecular geometry employed to describe the homo-oligomer; the small basis set for energy calculations; and the absence of both environmental and dynamical effects. In our opinion, the latter motives are probably the most important ones, and they can be overcome by using molecular dynamics (MD) simulation techniques.

In this work, we present a MD study about the conformational preferences of the $(\Delta Ala)_6$ homo-oligomer in dilute chloroform solution. We have used a 40-ns MD simulation including explicit solvent molecules to determine the stability of both the extended and 3_{10}-helix for this compound. Two different force-fields have been used in order to consider the geometry variation observed for the ΔAla residue with conformation [2]. Furthermore, in order to compare with experimental data, quantum mechanical calculations of the resulting structures have been performed to estimate ^{1}[H]-NMR chemical shifts. The resulting values have been compared with the values reported for *p*-BrBz–$(\Delta Ala)_n$–OMe.

2. Methods

2.1. Force-field calculations

MD simulations were run on a homo-oligomer chain of six ΔAla residues blocked at the N-terminus with an acetyl group and at the C-terminus with an *N*-methylamine group. Calculations were done using the SANDER module of Amber 4.1 [9], with a time step of 2 fs. The Berendsen temperature coupling method was used to keep the average temperature constant at 300 K using a coupling constant of 0.2 ps [10]. The OPLS chloroform model [11] was used for all solvent molecules, and the SHAKE algorithm [12] was used to constrain all bond-lengths to their equilibrium values. A 12-Å cutoff was used for the non-bonded interactions, i.e. if two residues or a residue and a chloroform molecule have any atom within 12 Å, the interaction between the entire pair is evaluated. The non-bonded pair list was updated every 25 MD steps.

All the force-field parameters, with exception of the atomic charges and some equilibrium geometrical parameters, were taken from the set of parameters explicitly developed for dehydroamino acids by Alagona and co-workers [13]. The atomic charges for the ΔAla residue were taken from our previous work, in which these electrostatic parameters were fitted to HF/6–31G(d) electrostatic potentials computed for the minimum energy conformations of the ΔAla-containing dipeptide [7]. The molecular geometries of the C_5 and α minima were also used to extract the equilibrium parameters involving the C^{α} atom [2]. Two sets of parameters were considered: (i) those in which the angle $<N-C^{\alpha}-C(O)$ presents a tetrahedral value, denoted force-field 1 (FF1); and (ii) those associated with the trigonal configuration of the C^{α}-atom in the α minimum, named force-field 2 (FF2). Table 1 shows the equilibrium parameters for the two force-fields. It can be seen that FF1 and FF2 only differ in the $N-C^{\alpha}$ bond length and the $N-C^{\alpha}-C(O)$ bond angle. This is because the remaining geometrical parameters are very similar

Table 1
Equilibrium geometrical parameters associated to the two force-fields (FF1 and FF2) used for ΔAla

	d(N–C$^{\alpha}$)	<N–C$^{\alpha}$–C
FF1	1.397	109.5
FF2	1.425	119.4

Bond lengths and angles are in Å and degrees, respectively.

for both the extended and helical conformations [2]. The starting conformations for the homo-oligomer were built considering $\varphi,\psi = 180°\ 140°$ (extended) and $\varphi,\psi = -40°,\ -30°$ (3_{10}-helix), in agreement with our previous studies [2,6].

A solvent box ($35.84 \times 35.85 \times 51.20$ Å^3) of 490 chloroform molecules (density = 1.47 g/cc) was created and equilibrated. The $(\Delta Ala)_6$ chain was centered in the solvent box and the overlapping chloroform molecules were removed. The resulting system contains 467 chloroform molecules and 1928 explicit atoms. During equilibration and subsequent MD simulations, periodic boundary conditions were applied.

The temperature of the system was slowly brought to 300 K by 24 ps of NVT-MD, i.e. increasing by 25 K every 2 ps. During this initial equilibration, the solvent molecules were restrained to their positions. After this, the energy of the system was equilibrated by performing 20 ps of NVT-MD, in which both the solvent molecules and the $(\Delta Ala)_6$ were allowed to move freely. Then, we conducted four simulations, i.e. extended and 3_{10}-helix conformations with FF1 and FF2, consisting of 10 ns each. Every 1 ps, the coordinates were saved on disk.

2.2. Quantum mechanical calculations

Some relevant conformations provided by MD simulations have been used to predict NMR properties of $(\Delta Ala)_6$. The electronic structure of these conformations was determined at the HF/6–311G(d) level [14].

Proton isotropic shielding constants of $(\Delta Ala)_6$, $\sigma(^1H_i)$, were computed using perturbation theory and the Gauge Invariant Atomic Orbitals (GIAO) method [15,16] implemented in the Gaussian 94 program package [17]. Chemical shifts, $\delta(^1H_i)$, are referred to a usual standard as TMS through the relation:

$$\delta(^1H_i) = \sigma(^1H_i)_{TMS} - \sigma(^1H_i)_{\Delta Ala6}$$

where, in order to have accurate chemical shifts, the isotropic shielding constant of hydrogen atoms in TMS, $\sigma(^1H_i)_{TMS} = 32.58$ ppm, was computed at the same level of calculation described above [18].

MD simulations were performed on a SGI Indigo^2 system with a single R10000 processor. Quantum mechanical calculations were performed at the Centre de Supercomputació de Catalunya (CESCA).

3. Results

First, we performed MD simulations of the extended conformation of $(\Delta Ala)_6$ using both FF1 and FF2 (MD_e/FF1 and MD_e/FF2, respectively). Fig. 1 shows the atom-positional root mean square deviation (RMSD) between the starting coordinates and the coordinates sequentially stored along 10-ns trajectories. Only the backbone atoms (N, C$^{\alpha}$ and C) were included when calculating the displayed RMSD. As can be seen, the fluctuations of the extended conformation are very small when the FF1 is used, the average RMSD along the trajectory being 0.67 ± 0.47 Å. Furthermore, fluctuations disappear almost completely after 5 ns of simulation. Fig. 2a shows the superposition of the peptide coordinates from 0.5 ns consecutive intervals. These results point out the high stability of the extended conformation for $(\Delta Ala)_6$ when the FF1 is used.

The RMSD for the structures resulting from the MD_e/FF2 simulation (Fig. 1b) indicates that the molecule preserves the extended conformation for approximately 5 ns. However, the partial fraying of two residues at the N-terminus induces a larger RMSD for MD_e/FF2 than for MD_e/FF1 along this period. The most remarkable feature of MD_e/FF1 corresponds to the change from the extended conformation to the 2_7-ribbon one at approximately 6 ns. This transition can be followed in Fig. 1b, which compares the RMSD from the starting extended conformation with that from a standard 2_7-ribbon one ($\varphi,\psi = +68.8°,\ -72.0°$). As can be seen, the RMSD from the last conformation is

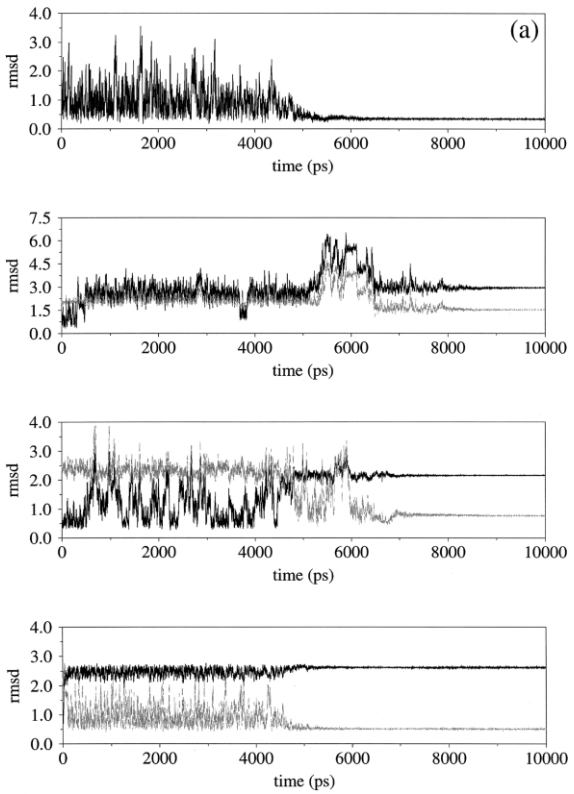

Fig. 1. Positional root-mean square deviation (RMSD; in Å) between the starting co-ordinates and the co-ordinates stored along 10 ns MD_e/FF1 (a), MD_e/FF2 (b), MD_h/FF1 (c) and MD_h/FF2 (d) trajectories of $(\Delta Ala)_6$. Only the backbone atoms were considered to obtain RMSD. For the MD_e/FF2, MD_h/FF1 and MD_h/FF2 trajectories (b, c and d), the RMSD of the saved coordinates with respect to the 2_7-ribbon conformation is also displayed (dashed lines).

small and almost constant along the last 3 ns of simulation, the average value during this period being 1.57 ± 0.16 Å. The extended-to-2_7-ribbon transition is shown in Fig. 2b, which displays some representative conformations extracted from MD_e/FF2 at periods ranging from 4.4 to 6 ns. Table 2 compares the final and average end-to-end distance for each simulation with the value of the starting conformation. As can be seen, this distance decreases by approximately 9 Å for MD_e/FF2, while for MD_e/FF1, it remains at approximately the same value.

Fig. 3 shows the number of intramolecular hydrogen bonds of C_5 type (O…H distance below 2.5 Å) during the MD_e/FF1 and MD_e/FF2 simulations. In the former trajectory, the six initial hydrogen bonds are retained, indicating that the extended conformation remains intact. However, only four hydrogen bonds remain formed in MD_e/FF2 at 5 ns and this number decreases to one at 6 ns. Fig. 3b also shows the number of intramolecular hydrogen bonds of C_7 type (seven-membered hydrogen bonded ring), which are characteristic of the 2_7-ribbon conformation. It should be noted that the amide groups at the N-terminus form C_7 interactions from the beginning of the MD_e/FF2 simulation, and the number of such interactions suddenly increases after 5 ns.

Fig. 4 displays the Ramachandran plots for the φ–ψ backbone dihedral angle pairs in ΔAla residues of $(\Delta Ala)_6$, extracted every 1 ps from the 10 ns MD_e/FF1 and MD_e/FF2 trajectories. The (φ–ψ pairs resulting from the MD_e/FF1 simulation are strictly confined to the extended region. There is no indication of strain in the φ–ψ angles when the FF1 is used. Fig. 4b also reflects the extended-to-2_7-ribbon conformational transition detected in MD_e/FF2. Thus, the two conformations are noticeably populated in Fig. 4b. Moreover, the scattering of the dihedral angle pairs from the extended to the 2_7-ribbon regions shows the route followed by the ΔAla residues during the transition.

MD simulations of the 3_{10}-helix using the FF1 and FF2 (MD_e/FF1 and MD_e/FF2, respectively) were performed in order to ascertain the stability of such conformation. In the former simulation, the starting 3_{10}-helix changes into a 2_7-ribbon in approximately 4.5 ns. Thus, the average RMSD with respect to the former conformation increases to 2.17 ± 0.10 Å after this period of time, while the average RMSD with respect to the latter decreases to 0.96 ± 0.48 Å (Fig. 1c). The reverse transition was not detected in the next 6.5 ns. The dynamics of the 3_{10}-helix-to-2_7-ribbon transition is illustrated in Figs. 5 and 6, which show a schematic picture of the structures extracted from different intervals and the number of hydrogen bonds for both conformations, respectively. Another view of such transition is provided in Fig. 4c, in which the distribution of the φ–ψ dihedral angle pairs points out that the change from the 3_{10}-helix to 2_7-ribbon occurs without visiting any

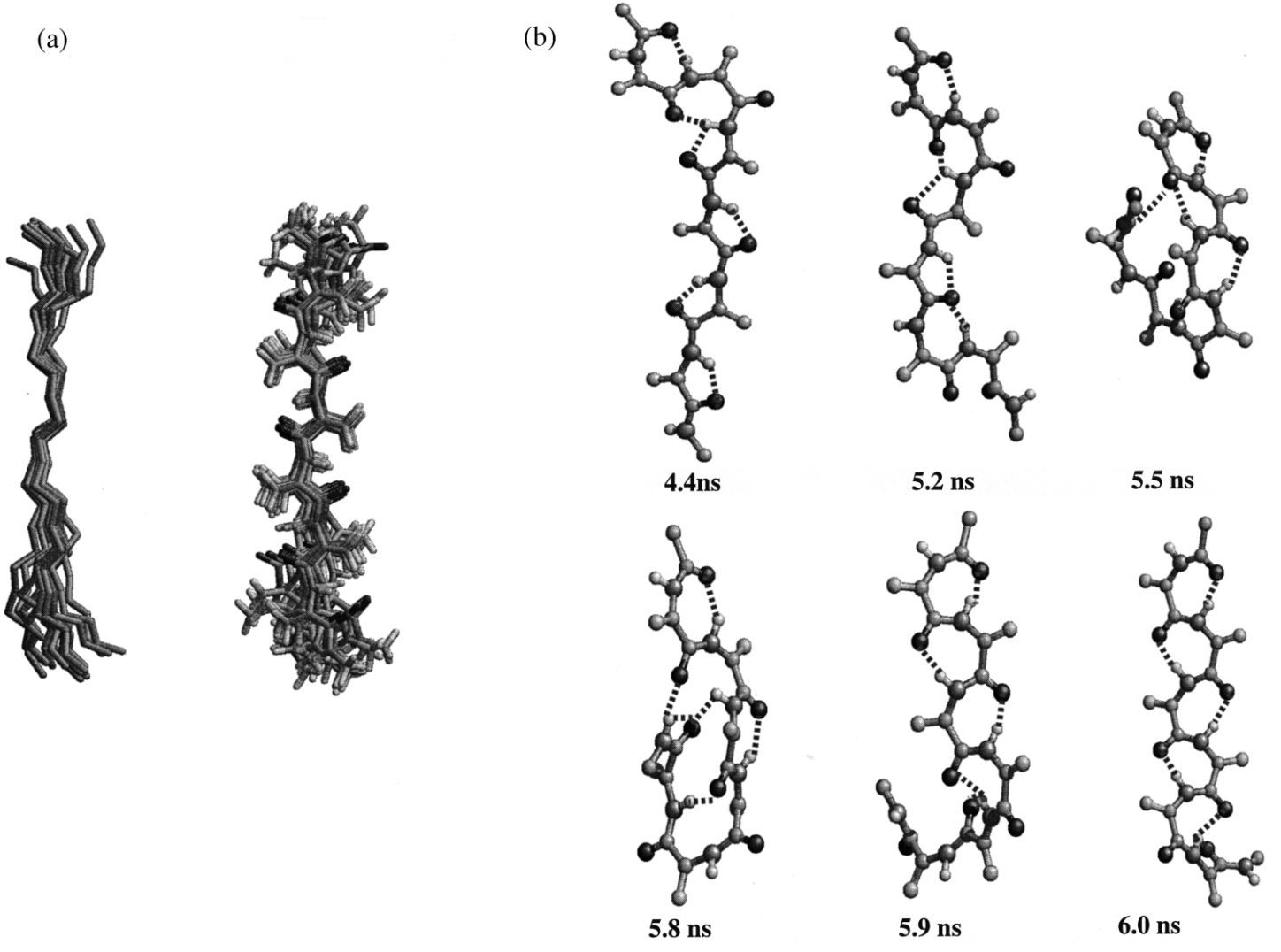

Fig. 2. (a) Superposition of $(\Delta Ala)_6$ coordinates from 0.5 ns consecutive intervals of MD_e/FF1. Both backbone atoms (left) and all atoms (right) are shown. (b) Representative snapshots from MD_e/FF2 of the extended-to-2_7-ribbon conformational transition of $(\Delta Ala)_6$. All the structures are depicted with the N-terminus up and the C-terminus down.

Table 2
End-to-end distance (Å) for the four MD simulations performed in this work

Simulation	Initial	Final	Average
MD_e/FF1	25.06	24.62	24.10 ± 0.94
MD_e/FF2	25.85	16.77	17.88 ± 3.13
MD_h/FF1	14.93	19.35	16.87 ± 2.38
MD_h/FF2	14.05	20.09	19.69 ± 0.89

Initial, final and average values are displayed.

intermediate conformation. The latter simulation was performed, considering a trigonal configuration for the C^{α} atom and a 3_{10}-helix as starting conformation (MD_e/FF2). In this case, the initial helical conformation quickly transforms into a 2_7-ribbon, the latter conformation remaining stable until the end of the simulation. This is reflected in the evolution of both the RMSD (Fig. 1d) and the number of intramolecular hydrogen bonds (Fig. 6b). The average RMSD with respect to the 3_{10}-helix and 2_7-ribbon conformations is 2.54 ± 0.14 and 0.73 ± 0.35 Å, respectively. On the other hand, the $i,i+3$ hydrogen bonds characteristic of the 3_{10}-helix, are completely broken and converted into interactions of the C_7 type after 45 ps of simulation. As can be seen in Table 2, the elongation of the molecular chain involved in the 3_{10}-helix-to-2_7-ribbon conformational transition is of approximately 6 Å.

Fig. 7a shows the evolution of the total potential energy for the four simulations: MD_e/FF1, MD_e/FF2, MD_h/FF1 and MD_h/FF2. As can be seen, in all cases, several nanoseconds are required for a complete equilibration of the energy. Obviously, this occurs later for MD_e/FF2 and MD_h/FF1 than for MD_e/FF1 and MD_h/FF2 because the conformational transitions of the formers appear at approximately half of the trajectories. The four simulations reach similar total energies after 10 ns of trajectory, MD_e/FF1 and MD_e/FF2 being slightly favored with respect to the others.

In order to provide a better description of the stability of the different conformations, we computed the peptide–peptide (p–p), peptide–chloroform (p–c) and chloroform–chloroform (c–c) interactions at the total trajectories. Results are displayed in Fig. 7b–d, respectively. It is worth noting that the extended conformation (MD_e/FF1) is the most favored conformation. Thus, the p–p intramolecular energy contribution is more favorable for such a conformation than for the 2_7-ribbon. On the other hand, the p–c and c–c intermolecular energy contributions are similar for the four simulations.

Toniolo and co-workers [8] found that the intramolecular interactions between the C^{β}–H^{β} and C=O groups of residues i and $i-1$, respectively, provide a significant contribution to the stability of the extended conformation. Thus, the $H_i^{\beta} \ldots O_{i-1}$ distance found by X-ray crystallography for *p*BrBz–$(\Delta Ala)_n$–OMe with $n=1$, 2 and 3 ranges from 2.25 to 2.45 Å. Furthermore, such compounds present an extended conformation in the solid state close to the standard one (φ, ψ = 180°, 180°) [8]. It should be noted that the formation of the $(C^{\beta}–H^{\beta})_i \ldots (O=C)_{i-1}$ six-membered hydrogen bonded rings (C_6) reinforces the stability provided by the $(N–H)_i \ldots (O=C)_i$ five-membered hydrogen bonded rings (C_5), the latter being characteristic of the ideally extended structures. However, the deviation of the backbone dihedral angles with respect to

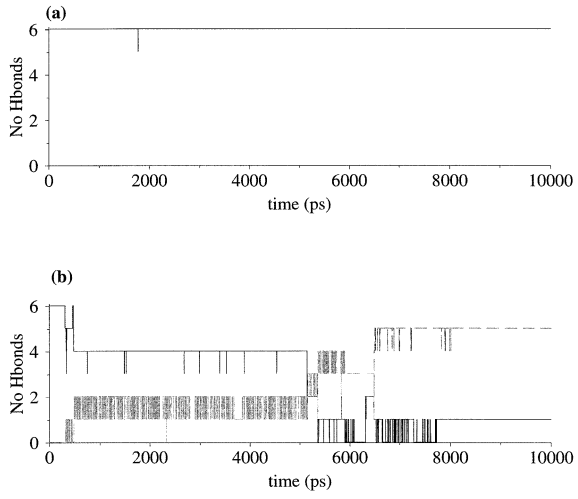

Fig. 3. Number of C_5 type intramolecular hydrogen bonds (O…H distance below 2.5 Å) during MD_h/FF1 (a) and MD_e/FF2 (b) simulations of $(\Delta Ala)_6$. The number of C_7 type hydrogen bonds are also displayed for the latter trajectory (dashed line).

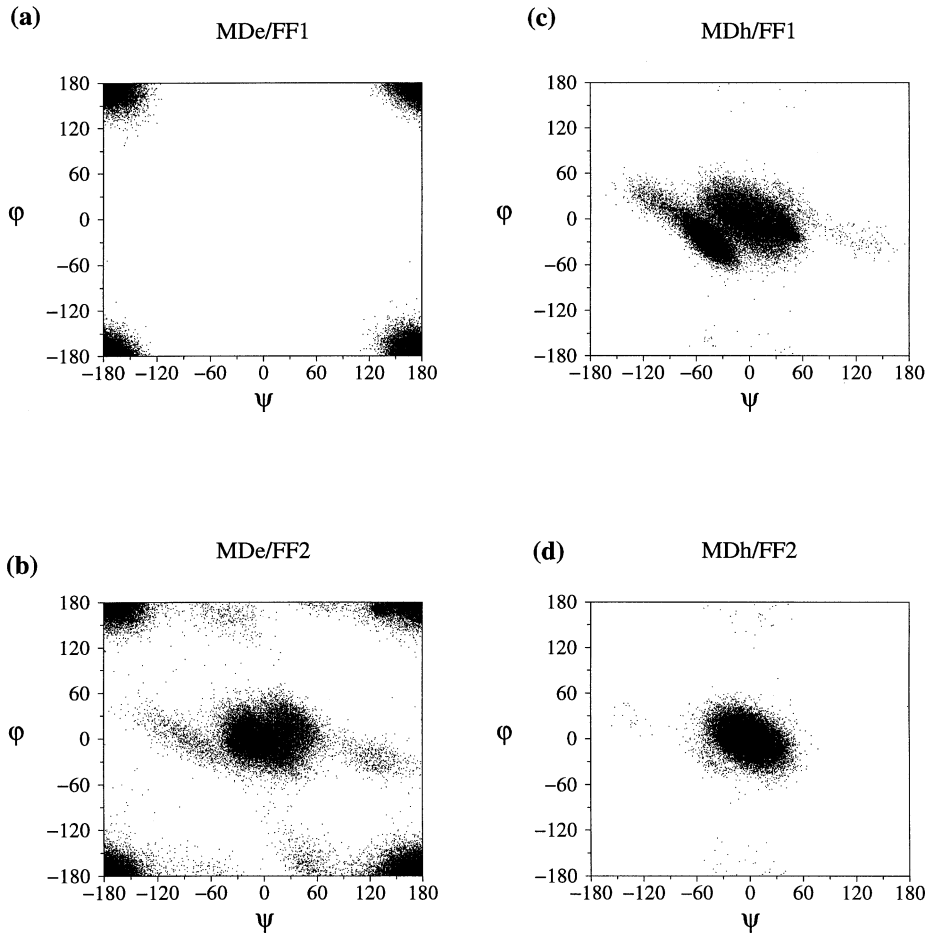

Fig. 4. Ramachandran plots showing φ and ψ dihedral angle pairs (in degrees) of ΔAla residues in $(\Delta Ala)_6$ every 1 ps: (a) MD_e/FF1; (b) MD_e/FF2; (c) MD_h/FF1; and (d) MD_h/FF2.

the ideal values observed in Fig. 6a may induce an enlargement of such distance in chloroform solution. This is a very reasonable result since, certainly, a small distortion of the solid state structure is expected in solution, where the packing effects are not present. Fig. 8 displays the number of $(C^{\beta}–H^{\beta})_i…(C=O)_{i-1}$ interactions with a $H_i^{\beta}…O_{i-1}$ distance lower than 2.9 Å as a function of the simulation time for MD_e/FF1. As can be seen, the number of residues involved in such interaction is approximately five. These results are in excellent agreement with the chemical shifts of the HO protons provided by Toniolo and coworkers for *p*BrBz–$(\Delta Ala)_6$–OMe in $CDCl_3$ solution. Thus, these authors attributed the deshielded resonances found for a half of the vinyl protons, i.e. one per residue, to the formation of intramolecular C–H…O=C interactions.

Finally, ab initio quantum mechanical calculations on $(\Delta Ala)_6$ were used to explore the differences in ^{1}[H]-NMR chemical shifts among the extended, 3_{10}-helix and 2_7-ribbon conformations. For this purpose, three conformers were selected from the 40-ns MD simulation. The extended conformation was taken from MD_e/FF1, the 3_{10}-helix from the first half of MD_h/FF1 and the 2_7-ribbon from MD_h/FF2. The proton chemical shifts evaluated for the three conformations at the HF/

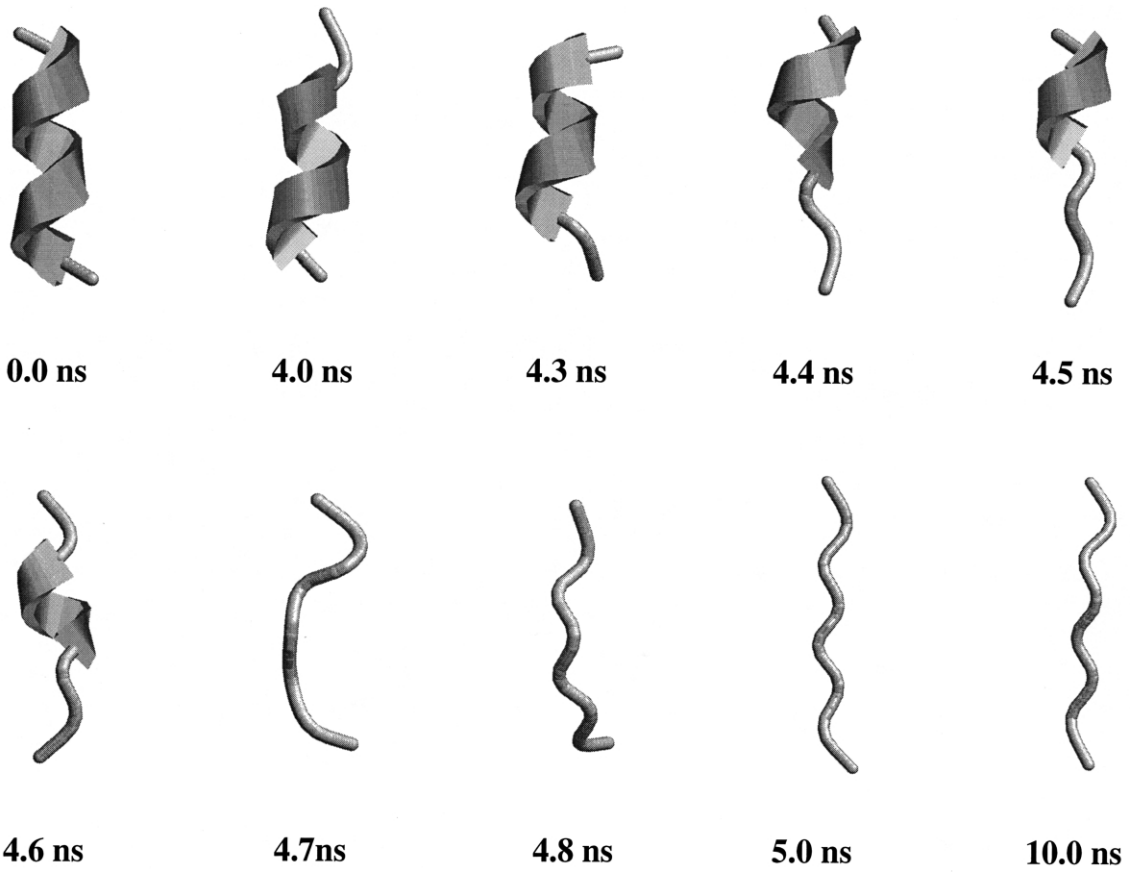

Fig. 5. Ribbon snapshots representing different consecutive intervals over the 10-ns MD_h/FF1 simulation of $(\Delta Ala)_6$. The molecules are depicted with the N-terminus up and the C-terminus down.

6-311G(d) level are displayed in Table 3, which also shows the experimental data obtained for *p*BrBz–$(\Delta Ala)_6$–OMe [8].

The best agreement between theoretical and experimental chemical shifts correspond to the 2_7-ribbon conformation. Thus, no correlation between experimental and theoretical data was found for the extended and 3_{10}-helix conformations. Conversely, the fitting ($y = cx$) between the experimental data and the values computed for the 2_7-ribbon conformation provides a Pearson correlation coefficient, *R*, of 0.84 and a scaling coefficient, *c*, of 0.93. Both the NH and $C^{\beta}H^{\beta}$ proton resonances are well reproduced for this conformation. On the other hand, in general, the $C^{\beta}H^{\beta}$ chemical shifts predicted for the extended conformation are in good agreement with experimental data, while the values provided by the 3_{10}-helix are underestimated. The NH chemical shifts are underestimated by approximately 2 ppm for these two conformations.

4. Discussion and remarks

Results indicate the crucial role of the force-field on MD simulations of ΔAla oligopeptides. It should be noted that the two force-fields used in this work, FF1 and FF2, only differ in some equilibrium geometrical parameters. The main difference concerns the $<N-C^{\alpha}-C$ angle, which is lower than the standard trigonal bond angle of 120° for FF1, and close to such value for FF2. Indeed, FF1 and FF2 are based on the conforma-

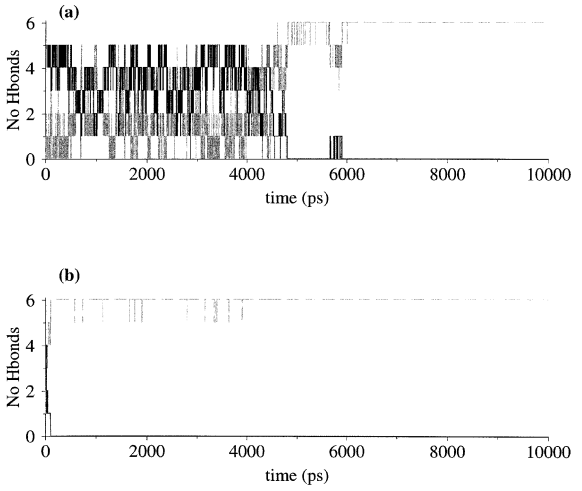

Fig. 6. Number of both $i,i+3$ (solid line) and C_7 (dashed line) intramolecular hydrogen bonds characteristic of the 3_{10}-helix and 2_7-ribbon conformations, respectively, during the MD_h/FF1 (a) and MD_h/FF2 (b) simulations of $(\Delta Ala)_6$.

tional dependence predicted by quantum mechanical calculations for the ΔAla dipeptide [2], the parameters of the former and the latter force-fields being those of the extended and helical minimum energy conformations, respectively. It should be noted that the $<N-C^{\alpha}-C$ angle found by X-ray crystallography for the extended conformation of the ΔAla residue (110°) is greatly narrowed compared to that typical of a trigonal sp^2-hybridized atom. This is in good agreement with our previous quantum mechanical calculations [2] and suggests that the results achieved using the FF1 are the most reliable for this study.

The extended conformation, which was experimentally detected for *p*BrBz–$(\Delta Ala)_6$–OMe [8], only remains stable when the FF1 is used. The FF2 induces an extended-to-2_7-ribbon conformational transition. On the other hand, the 3_{10}-helix evolves towards a 2_7-ribbon in all cases, the transition being extremely fast for FF2. The 2_7-ribbon consists of the repetitive sequence of C_7 interactions. It should be mentioned that the $<N-C^{\alpha}-C$ angle for the C_7 conformation of ΔAla-containing dipeptide was 120.8° [2]. Quantum mechanical calculations on $(\Delta Ala)_6$ predicted that the 2_7-ribbon conformation is less favored than the extended and 3_{10}-helix ones by 4.0 and 2.2 kcal/mol in the gas-phase [6]. The results obtained in the present work indicate that dynamical and solvent effects, which were not included in our previous energy minimization study [6], play a very important role on the conformational preferences of ΔAla oligopeptides.

On the other hand, the differences found among the simulations performed with FF1 and FF2 point out the intrinsic limitations of the techniques based on molecular mechanics. Thus, the conformational dependence of both bond lengths and bond angles are usually neglected in studies based on classical potentials, in which these equilibrium geometric parameters remain constant for all the conformations. This can be an important source of error in conformational studies of peptides constituted by non-standard residues, in which the $<N-C^{\alpha}-C$ angle is considered as conformationally indicative [19]. The results presented in this work clearly reflect that a bad choice of an equilibrium geometric parameter can lead to erroneous results. Thus, caution must be taken to study, with conventional MD techniques, conformational transitions involving large changes in the geometrical parameters, such as, for instance, the extended-to-3_{10}-helix transition of $(\Delta Ala)_n$ homopeptides.

From a dynamical point of view, two common features are detected in the extended-to-2_7-ribbon and 3_{10}-helix-to-2_7-ribbon conformational transitions. The first one is that in both cases the transition occurs spontaneously, i.e. no potential function to force them was used. The second one is that the conformational changes are quite fast, and therefore, no stable intermediate state was found. However, the paths followed in the extended-to-2_7-ribbon and 3_{10}-helix-to-2_7-ribbon transitions are clearly displayed in Fig. 4b,c, respectively.

Analysis of the intramolecular p–p energy contributions indicates that the extended conformation obtained with the FF1 is more stable than the 2_7-ribbon achieved with the same force-field, even though the energy of the two arrangements become similar when the p–c and c–c contributions are considered. These results are in good agreement with those previously obtained using quantum mechanical calculations [6]. Thus, the extended

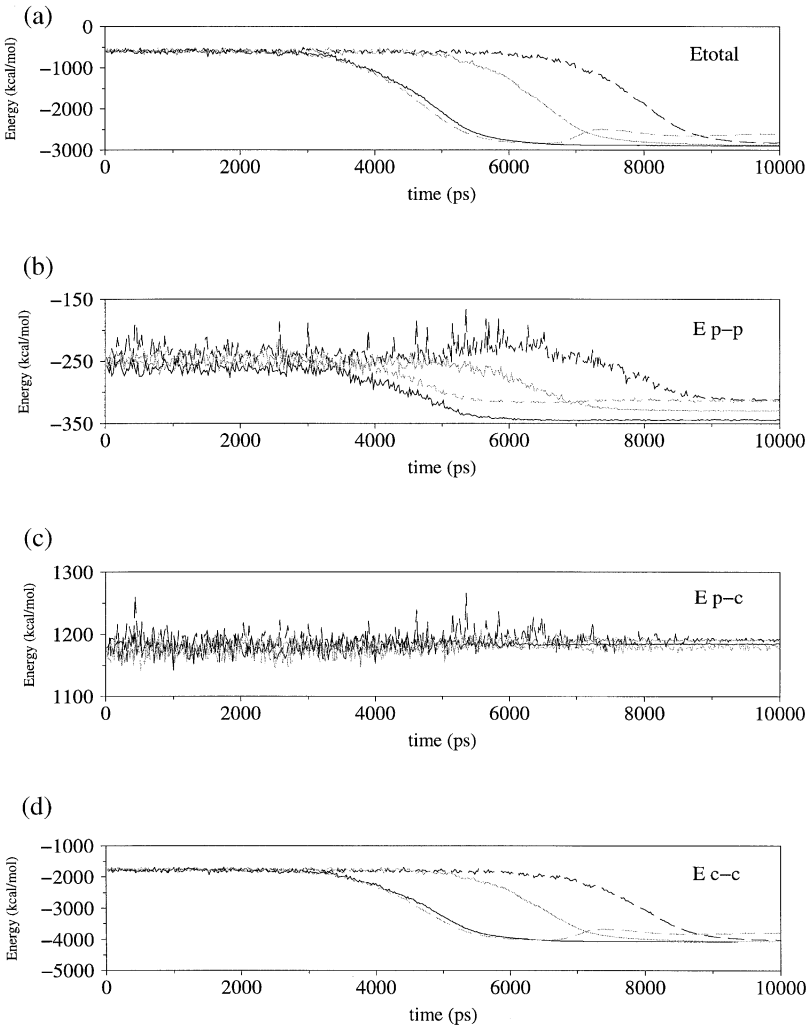

Fig. 7. Evolution of the total energy (a), the peptide–peptide (b), the peptide–chloroform (c) and the chloroform–chloroform (d) energies through the MD_e/FF1 (solid black line), MD_e/FF2 (dashed black line), MD_h/FF1 (solid gray line) and MD_h/FF2 (dashed gray line) simulations of $(\Delta Ala)_6$.

conformation was predicted to be the most favored conformation for homopeptides with a small number of residues. Moreover, they are consistent with the equilibrium geometric parameters experimentally observed for the extended conformation [8]. Thus, Toniolo and co-workers evidenced by ^{1}[H]-NMR and FTIR absorption techniques that the extended conformation predominates for short homopeptides ($n \geq 6$) in chloroform solution [8].

^{1}[H]-NMR chemical shifts were computed for the extended, 2_7-ribbon and 3_{10}-helix conformations at the HF/6-311G(d) level using the GIAO method. Chemical shifts predicted for the extended conformation are not in complete agreement with the experimental data reported by Toniolo and co-workers [8]. Thus, the $C^{\beta}H^{\beta}$ chemical shifts are well reproduced, but the NH proton resonances are poorly described. On the other hand, the chemical

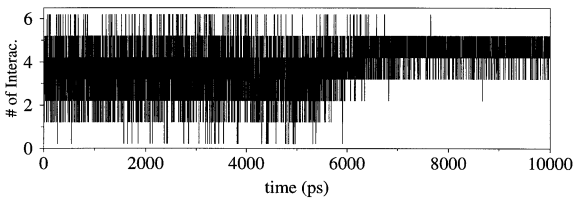

Fig. 8. Evolution of the number of $(C^{\beta}H^{\beta})_i \ldots (C{=}O)_{i-1}$ interactions through the MD_e/FF1 simulation. An interaction was considered as formed when the $H_i^{\beta} \ldots O_{i-1}$ distance was less than 2.9 Å.

shifts predicted for the 2_7-ribbon conformation fit quite well with experimental data, not only qualitatively but also quantitatively. These results suggest that $(\Delta Ala)_6$ presents an equilibrium between fully and partially extended conformations. Thus, some of the C_5 systems of the fully extended conformation could change to C_7 by short periods of time.

Acknowledgments

The authors thank the Centre de Supercomputació de Catalunya (CESCA) for computational facilities. The authors also wish to acknowledge helpful correspondence with Prof. C. Toniolo.

Table 3
Comparison among the theoretical chemical shifts (in ppm) of ^{1}[H] estimated for the extended, 3_{10}-helix and 2_7-ribbon conformations of $(\Delta Ala)_6$

Residue #	Exp.	Extended	3_{10}-Helix	2_7-Ribbon
1 Amide NH	8.86	5.90	4.67	5.19
Vinyl $C^{\beta}H^{\beta}$	6.80, 5.53	6.26, 5.41	6.11, 4.89	5.94, 4.94
2 Amide NH	8.97	6.36	4.74	8.87
Vinyl $C^{\beta}H^{\beta}$	6.67, 5.57	6.26, 6.10	5.45, 4.98	5.92, 5.77
3 Amide NH	8.95	6.74	8.20	8.44
Vinyl $C^{\beta}H^{\beta}$	6.67, 5.57	6.76, 5.66	5.05, 4.99	5.81, 6.16
4 Amide NH	8.95	7.17	7.21	8.99
Vinyl $C^{\beta}H^{\beta}$	6.66, 5.56	6.77, 6.02	5.20, 5.05	6.26, 6.10
5 Amide NH	8.95	6.82	7.60	8.64
Vinyl $C^{\beta}H^{\beta}$	6.66, 5.55	6.50, 5.60	5.74, 4.93	5.50, 5.60
6 Amide NH	8.56	7.88	7.32	8.64
Vinyl $C^{\beta}H^{\beta}$	6.65, 6.04	7.06, 5.14	5.64, 5.33	5.85, 5.34

Experimental values measured for *p*BrBz–$(\Delta Ala)_6$–OMe are also included.

References

[1] T.P. Singh, P. Kaur, Conformation and design of peptides with α,β-dehydro-amino acid residues, Prog. Biophys. Molec. Biol. 66 (1996) 141–165.
[2] C. Alemán, J. Casanovas, Molecular conformational analyses of dehydroalanine analogues, Biopolymers 36 (1995) 71–82.
[3] M. Thormann, H.-J. Hofmann, Conformational properties of peptides containing dehydro amino acids, J. Mol. Struct. (Theochem) 431 (1998) 79–96.
[4] C. Alemán, J.J. Pérez, A conformational study of the dehydroalanine: dipeptide and homopolypeptide, Biopolymers 33 (1993) 1811–1817.
[5] P. Fabian, V.S. Chauhan, S. Pongor, Biochim. Biophys. Acta 1208 (1994) 89, ESTE.
[6] J. Casanovas, C. Alemán, A quantum-mechanical study of the chain-length dependent stability of the extended and 3_{10}-helix conformations in dehydroalanine oligopeptides, J. Comput. Aided Mol. Design 8 (1994) 441–448.
[7] C. Alemán, Effect of the environment and the role of the π–π stacking interactions in the stabilization of the 3_{10}-helix conformation in dehydroalanine oligopeptides, Int. J. Peptide Protein Res. 46 (1995) 408–419.
[8] M. Crisma, F. Formaggio, C. Toniolo, T. Yoshikawa, T. Wakamiya, Flat peptides, J. Am. Chem. Soc. 121 (1999) 3272–3278.
[9] D.A. Pearlman, D.A. Case, J.W. Caldwell, et al., AMBER v. 4.1, University of California, San Francisco, CA, USA, 1995.
[10] H.J.C. Berendsen, J.P.M. Postman, W.F. van Gunsteren, A. DiNola, J.R. Haak, Molecular dynamics with coupling to an external bath, J. Chem. Phys. 81 (1984) 3684–3690.
[11] W.L. Jorgensen, J.M. Briggs, J.L. Contreras, Relative partition coefficients for organic solutes from fluid simulations, J. Phys. Chem. 94 (1990) 1683–1686.
[12] J.-P. Ryckaert, G. Ciccotti, H.J.C. Berendsen, Numerical integration of the Cartesian equations of motion of a system with constraints: molecular dynamics of *n*-alkanes, J. Comput. Phys. 23 (1977) 327–341.
[13] G. Alagona, C. Ghio, C. Pratesi, Force-field parameters for molecular mechanical simulation of dehydroamino acid residues, J. Comput. Chem. 8 (1991) 934–942.
[14] A.D. McLean, G.S. Chandler, Contracted Gaussian basis sets for molecular calculations. 1. Second row atoms, $Z=11$–18, J. Chem. Phys. 72 (1980) 5639–5648.
[15] R. Ditchfield, Molecular orbital theory of magnetic shielding and magnetic susceptibility, J. Chem. Phys. 56 (1972) 5688–5691.

[16] K. Wolinski, J.F. Hinton, P. Pulay, Efficient implementation of the gauge-independent atomic orbital method for NMR chemical shifts calculations, J. Am. Chem. Soc. 112 (1990) 8251–8260.
[17] M.J. Frisch, H.B. Trucks, H.B. Schlegel, et al., Gaussian 94, Revision B.3, Gaussian, Inc, Pittsburgh PA, 1995.
[18] J. Casanovas, G. Pacchioni, F. Illas, Si solid state NMR of hydroxyl groups on silica from first principle calculations, Mater. Sci. Eng. B 68 (1999) 16–21.
[19] E. Benedetti, in: B. Weinstein (Ed.), Chemistry and Biochemistry of Amino Acids, Peptides and Proteins, Vol 6, Dekker, New York, 1983, pp. 105–184.